Equivalence of the freely cooling granular gas to the sticky gas

Mahendra Shinde,[1,*] Dibyendu Das,[1,†] and R. Rajesh[2,‡]
[1]*Department of Physics, Indian Institute of Technology, Bombay, Powai, Mumbai-400 076, India*
[2]*Institute of Mathematical Sciences, CIT campus, Taramani, Chennai-600113, India*
(Received 31 October 2008; published 11 February 2009)

A freely cooling granular gas with a velocity-dependent restitution coefficient is studied in one dimension. The restitution coefficient becomes near elastic when the relative velocity of the colliding particles is less than a velocity scale δ. Different statistical quantities, namely, density distribution, occupied and empty cluster length distributions, and spatial density and velocity correlation functions, are obtained using event driven molecular dynamic simulations. We compare these with the corresponding quantities of the sticky gas (inelastic gas with zero coefficient of restitution). We find that in the inhomogeneous cooling regime, for times smaller than a crossover time t_1, where $t_1 \sim \delta^{-1}$, the behavior of the granular gas is equivalent to that of the sticky gas. When $\delta \to 0$, then $t_1 \to \infty$ and, hence, the results support an earlier claim that the freely cooling inelastic gas is described by the inviscid Burgers equation. For a real granular gas with finite δ, the existence of the time scale t_1 shows that, for large times, the granular gas is not described by the inviscid Burgers equation.

DOI: 10.1103/PhysRevE.79.021303 PACS number(s): 45.70.Mg, 47.70.Nd, 05.70.Ln

I. INTRODUCTION

Granular systems, ubiquitous in nature, exhibit a wide variety of physical phenomena [1,2]. The nonequilibrium nature of these systems, characterized by dissipative particle collisions and external driving, has attracted a lot of attention from the theoretical point of view [3]. However, analytical progress remains slow. It is therefore important to understand completely simple models that capture some essential feature of these systems.

A simple well studied model that captures dissipation effects is freely cooling gas wherein particles at high temperature come to rest through inelastic collisions [4–23]. At short times, the particles undergo homogeneous cooling, described by the Haff's law [24], wherein the kinetic energy of the system decreases with time t as t^{-2}. This behavior has recently been verified experimentally [25]. Beyond a crossover time t_c, the system crosses over to the inhomogeneous cooling state, characterized by clustering, where the energy decays according to a different power law $\sim t^{-\psi}$. The exponent ψ is dependent on dimension. For instance, $\psi = 2/3$ in one dimension and $\psi \approx 1$ in two dimensions.

In one dimension, it has been possible to make considerable analytic and numerical progress. In the special case when the coefficient of restitution (henceforth denoted by r) is zero, i.e., particles stick on collision, the problem is exactly solvable. The problem can be mapped on to the description of shocks in velocity field in the inviscid Burgers equation [4]. Burgers equation being exactly solvable in one dimension [26], the exact expressions for different quantities such as velocity distribution, mass distribution, and energy decay as a function of time are known. This limit ($r=0$) will be referred to as the sticky gas. In this paper, we will refer to the case $0 < r < 1$ as granular gas.

Extensive simulations of granular gas in one dimension showed that, beyond the crossover time t_c, the energy decay in the granular gas is identical to that of sticky gas [5]. Not only is the exponent ψ the same, all the curves for different r's collapse on top of each other. In addition, the velocity distribution was seen to be independent of r. Finally, the coarsening length scale $\mathcal{L}(t)$ scaled with t identically for both granular and sticky gas. It was thus concluded that the long time behavior ($t > t_c$) of granular gas is described by the Burgers equation. This analogy was generalized to higher dimensions in Ref. [6], though its applicability remains unclear [17].

To make this equivalence in one dimension stronger, the two point correlations of the granular and the sticky gases need to be compared. In a recent paper [27] we showed that, when r depends on the relative velocity, there is a new crossover time t_1 (with $t_1 > t_c$), beyond which the coarsening properties of granular gas differ from that of sticky gas or the Burgers equation. This was shown numerically by measuring the spatial density-density and velocity-velocity correlation functions. In this paper, we focus on the intermediate time $t_c < t < t_1$, and show that the correlation functions of granular gas compare well with that of sticky gas, obeying what is known as the Porod law. In Sec. II, we review this law in the context of coarsening systems, and point out some nonequilibrium systems where it is known to be violated.

Our study involves event driven molecular dynamics simulations of granular and sticky gases on a ring. The precise definition of the model and the definition of the statistical quantities that we measure are presented in Sec. III. The quantities that will be studied are density distributions, density-density and velocity-velocity correlation functions, and size distribution of empty and occupied clusters.

Modeling the coefficient of restitution r is crucial in defining the model and understanding cooling granular gases. Experimentally, it is known that r tends to 1 (elastic limit) when the relative velocity of collision decreases to zero [28–30], while for large relative velocities r tends to a constant. This introduces a velocity scale δ in the problem,

*shinde_m_l@iitb.ac.in
†dibyendu@phy.iitb.ac.in
‡rrajesh@imsc.res.in

which consequently gives rise to a new time scale t_1. As in Ref. [27], we model r as

$$r = (1 - r_0)\exp(-|v_{\rm rel}/\delta|^{\sigma}) + r_0, \quad (1)$$

where δ represents a velocity scale, below which collisions become near elastic, i.e., when the relative velocity $v_{\rm rel} \ll \delta$, then $r \to 1$ (elastic collision). For $v_{\rm rel} \gg \delta$ the collisions are inelastic with $r \to r_0$. The parameter σ decides how abruptly this crossover occurs. For example, for $\sigma \to \infty$, r versus $v_{\rm rel}$ is a step function while for finite σ it is a smoother curve. For $\sigma < 1$, the curve has a cusp as it approaches $r=1$. The experimental curves [28] suggest that the power σ can vary over wide range. Within the framework of viscoelastic theory, a power of $\sigma = 1/5$ has been predicted [31,32]. Apart from that, studies of velocity distribution in freely cooling granular gases with velocity-dependent restitution coefficient have been done using techniques different from that in this paper, namely, direct simulation Monte Carlo and viscoelastic theories [33,34]. With $\sigma \to \infty$ and δ held finite, our problem becomes the same as the granular gas problem studied earlier in Ref. [5].

The existence of a new crossover time t_1 was briefly shown in our earlier publication [27]. In Sec. IV, we present simulation results, showing explicitly the existence of t_1 for different δ and σ and determine its dependence on δ and σ. We then proceed to do a detailed comparison of the early time behavior of the granular gas and the sticky gas in Sec. V. We do the comparison on the basis of data for the various statistical quantities characterizing coarsening in these systems. In Sec. VI, the two point correlations are related to the empty and occupied cluster distributions through a mean-field approximation. This derivation leads us analytically to the Porod law for these coarsening systems. Conclusions and discussions are presented in Sec. VII.

II. THE POROD LAW

The freely cooling granular gas is an example of what is known as a coarsening or a phase ordering system. It is well known that in systems freely relaxing to ordering states, there exists a length scale $\mathcal{L}(t)$ that increases with time [35]. In addition, for usual phase ordering systems, the presence of a dominant $\mathcal{L}(t)$ results in a robust scaling law called the Porod law [35,36]. For scalar order parameters, the Porod law states that in d dimensions, the scaled structure function $S(k,t)/\mathcal{L}^d \sim (k\mathcal{L})^{-\theta}$ for large $k\mathcal{L}$, with $\theta = d+1$. Hence, in one dimension $\theta = 2$. In the above, $S(k,t)$ is the Fourier transform of the two-point correlation function of the order parameter. We shall refer to systems having the above features as clean phase ordering systems. The essential fact is that, in clean phase ordering systems the relative fluctuation with respect to the ordered state is nominal. For example, in the case of a ferromagnetic Ising model, a finite system at infinitely large time shows magnetization per site peaked at two possible values of spontaneous magnetization.

A few nonequilibrium systems, e.g., particles sliding on a randomly fluctuating surface [37–39], active nematics, namely, agitated granular-rod monolayers or films of orientable amoeboid cells [40], show a different kind of phase ordering; the main characteristic of which is undamped relative fluctuations even in the thermodynamic limit. Hence, it is called fluctuation dominated phase ordering. In such systems strong fluctuations sustain in time without losing macroscopic order. The order parameters have broad probability distributions even in the thermodynamic limit indicating strong variation of the order parameter in time. Unlike usual phase ordering, there need not be sharp interfaces distinguishing one phase from the other. The ensemble-averaged spatial correlation function shows a scaling form in $|r/\mathcal{L}(t)|$, but unlike clean phase ordering systems, it exhibits either a cusp or a power law divergence at small values of $|r/\mathcal{L}(t)|$. Hence the scaled structure factor varies as $S(k,t)/\mathcal{L}^d \sim (k\mathcal{L})^{-\theta}$ with $\theta < 2$. Thus, measuring θ is a reliable test to identify deviations from the Porod law.

We recently showed that the freely cooling granular gas at large times ($t > t_1$) also shows fluctuation dominated phase ordering [27]. The spatial correlation function shows a power law divergence for small values of $|r/\mathcal{L}(t)|$. This in turn indicates violation of the Porod law in the density and velocity structure functions with $\theta \approx 0.8$ [27]. The Porod law violation here indicates the presence of power law distributed clusters. In other words, the phase ordering is not clean. Earlier, in a slightly different model in one dimension with velocity-dependent restitution coefficient [41], it was found that the coarsening clusters are not long lived and they start breaking up at late times. That result seems to have similarity to what we found in Ref. [27] at late times $t > t_1$. But interestingly we find that at late times ($t > t_1$) there are two subregimes, namely, $t_2 > t > t_1$ and $t > t_2$. Here $t_2 \sim \delta^{-3}$ [5] is the very large scale beyond which all collisions become elastic and the system again becomes homogeneous. On the other hand, the regime $t_2 > t > t_1$ is the new and nontrivial regime of "unclean" ordering that we have found [27] and are highlighting here.

For Burgers equation, it was shown numerically in Ref. [13] (also see Sec. V), that the ordering is clean phase ordering, such that Porod law is obeyed. In this paper we examine the structure factor for the granular gas for intermediate times and show that Porod law is obeyed, as in the sticky gas.

III. THE MODEL

In this section, we define the model and the different physical quantities that are measured. Consider N point particles of equal mass on a ring of length L. Initially, the particles are distributed randomly in space with their velocities drawn from a normal distribution. Choose the reference frame in which the center of mass momentum is zero. The particles undergo inelastic, momentum conserving collisions such that when two particles i and j with velocities u_i and u_j collide, the final velocities u_i' and u_j' are given by

$$u_{i,j}' = u_{i,j}\left(\frac{1-r}{2}\right) + u_{j,i}\left(\frac{1+r}{2}\right), \quad (2)$$

where the relative velocity-dependent restitution coefficient r is given by Eq. (1). For sticky gas, $\delta = 0$ and $r_0 = 0$, such that

$r=0$ for all collision velocities, and the particles coalesce on collision.

For both systems, granular gas ($0<r_0<1$) and sticky gas ($r=0$), we have done event driven molecular dynamics simulations with system size $L=20\,000$ in units of the mean interparticle spacing at time $t=0$. The particle density is set to 1 throughout. Periodic boundary conditions were imposed. For the granular gas, simulations were performed for $r_0=0.1$, 0.5, and 0.8 in the time regime in which $\mathcal{L}(t)\ll L$. Thus, formally the sequence of limits are $L\to\infty$ first and then $t\to\infty$. In such a regime, the system continually coarsens, and hence we refer to it as a "phase ordering system." In this time regime, simulations were done for various different values of σ (namely, 3, 4, 5, 10, and ∞) and δ (namely, 0.001, 0.002, and 0.004). We found no qualitative variation of our main results with varying values of r_0, σ, and δ. Therefore, unless otherwise specified, the data that is presented for the granular gas corresponds to $r_0=0.5$, $\sigma=3.0$, and $\delta=0.001$.

It is well known that for $\delta=0$, event driven molecular dynamics simulations cannot go beyond the inelastic collapse. A similar difficulty is faced when δ is finite, but $\sigma\to 0$. For example, doing simulation with realistic σ such as $1/5$ (suggested from viscoelastic theories) or $1/4$ (for plastic collisions at large velocities), is out of our reach. At such small σ the shape of the r versus $v_{\rm rel}$ curve has a cusp as $v_{\rm rel}\to 0$. The particles practically do not see an elastic regime and the simulation run into difficulties such as particle overlap and inelastic collapse. Nevertheless, from our studies of $\langle\rho^2\rangle$ versus t (Fig. 3), we see that with decreasing σ the "clean phase ordering regime" gets extended further in time. So we hope this trend would continue even for smaller σ that our simulation could not access. Also, the exponents are independent of the σ values that we have studied, and we hope this trend will hold for smaller σ too.

The primary difference between a sticky gas and an granular gas is that in the former particles coalesce to form larger and larger mass clusters, while in the latter masses never coalesce. As a result, "clustering" phenomena in granular gas can be meaningfully quantified only if we define a local coarse-grained mass density ρ. To do so, first divide the ring into equally sized N boxes. For the granular gas, ρ_i is defined to be the total number of particles in the ith ($i=1,2,3,\ldots,N$) box. The coarse grained velocity v_i is defined as the mean of the velocities of all the particles in box i.

We now define the statistical quantities that are measured for the granular gas. The extent of clustering can be measured in terms of the variation of the density distribution $P(\rho,t)$. It is the probability of finding a spatial box with density ρ at time t. The first moment $\langle\rho\rangle(t)$ of the distribution $P(\rho,t)$ is constant at all times as the total mass is a conserved quantity. The second moment $\langle\rho^2\rangle(t)$, is defined in our simulation as $\langle\Sigma_i\rho_i^2\rangle/N$, where the sum is over all the boxes at time t and the average $\langle\cdots\rangle$ is over initial conditions.

Other measures of clustering are the cluster lengths and gap lengths. The distribution $O(x,t)$ is the number of clusters with exactly x successive occupied boxes at time t, normalized by the total number of occupied clusters. Likewise, the distribution $E(x,t)$ is the number of clusters with exactly x successive empty boxes at time t, normalized by the total number of empty clusters.

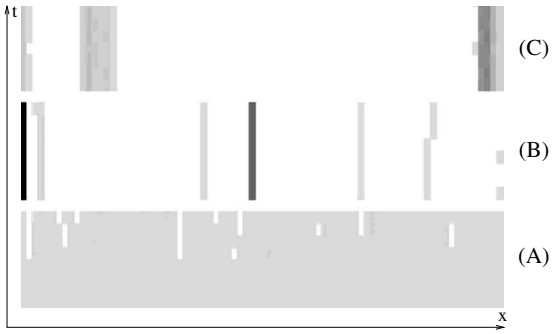

FIG. 1. The spatial density distribution is shown for different time regimes: (a) $t=0-7$ ($t\ll t_c$), (b) $t=600-607$ ($t_c<t<t_1$), and (c) $t=8000-8007$ ($t\gg t_1$). The darker regions correspond to higher densities. The data is for the granular gas with $r=0.5$, $\delta=0.004$, and $\sigma=\infty$. For these values of the parameters $t_1\simeq 1500$.

The other quantities of interest in this paper are spatial correlation functions. The equal time, two-point density-density spatial correlation function is defined as $C_{\rho\rho}(x,t)=\langle\rho_i(t)\rho_{i+x}(t)\rangle$, where ρ_i and ρ_{i+x} are densities at box i and box $(i+x)$, respectively. The structure function $S_{\rho\rho}(k,t)$ is the Fourier transform of $C_{\rho\rho}(x,t)$. Similarly, the equal time, two-point velocity-velocity spatial correlation function is defined as $C_{vv}(x,t)=\langle v_i(t)v_{i+x}(t)\rangle$, where v_i and v_{i+x} are the coarse grained velocities of box i and box $(i+x)$, respectively. The structure function $S_{vv}(k,t)$ is the Fourier transform of $C_{vv}(x,t)$.

In comparison to the granular gas, as particles coalesce in a sticky gas, they form bigger and bigger mass clusters localized at points in space, such that their total number steadily decreases with time. Therefore, without coarse graining, one can measure mass and velocity distribution functions, and the corresponding two-point correlation functions in space. But, to maintain uniformity with the granular gas, we will continue to use coarse grained densities and velocities for the sticky gas.

IV. THE NEW CROSSOVER TIME t_1

In this section, we show that the introduction of a velocity scale δ introduces a new time scale t_1, beyond which the granular gas deviates from the usual clean phase ordering as seen in sticky gas. We first show the different coarsening regimes by means of a space-time density plot. In Fig. 1, the density distribution is shown for three different time regimes with the darker regions corresponding to higher density.

In Fig. 1(a), we show a snapshot of the density profile of the system in a finite portion of space for few successive time steps, for very early times, $t\ll t_c$. We see that the system is fairly homogeneous. In Fig. 1(b), a similar plot of the density profile is shown for intermediate times $t_c<t<t_1$. The picture looks similar to any ordinary clean phase ordering system with steady growth of isolated large density lumps (deep dark shaded), along with large empty gaps (white) separating them. If the clean phase ordering continues, then at later times one would expect one or two very huge lumps remaining. Instead, in Fig. 1(c), we find grey shaded spatially

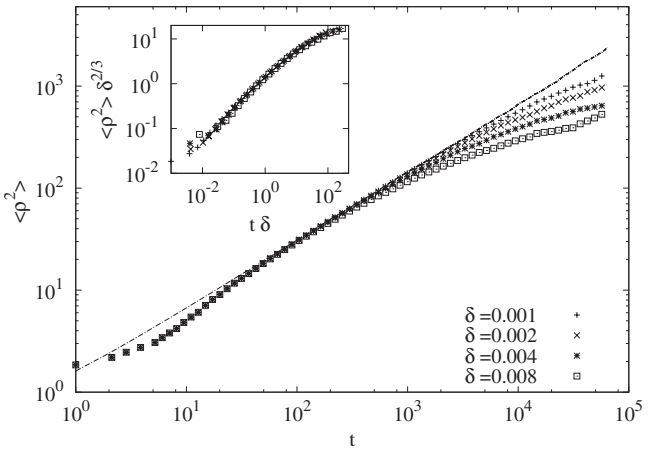

FIG. 2. The temporal variation of the second moment of density $\langle\rho^2\rangle$ for the granular gas is shown for different values of δ with $\sigma=3$ for all the cases. The data is for the granular gas except for the dotted line which corresponds to the sticky gas. The dotted line varies as $t^{2/3}$. The data for the granular gas coincides with that of the sticky gas for intermediate times, before deviating. The inset shows data collapse for various δ when the variables are scaled as in Eq. (3).

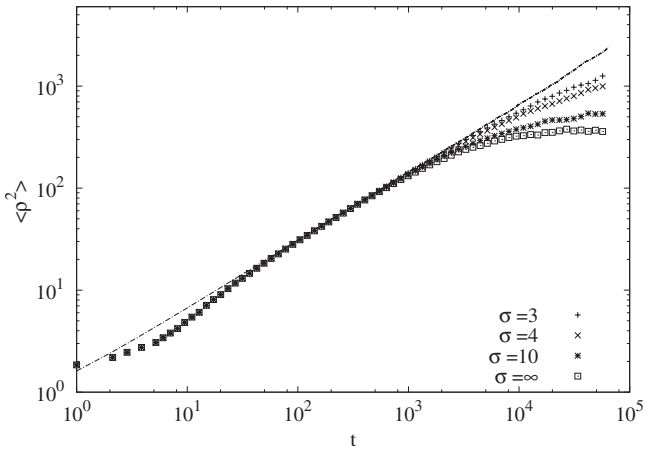

FIG. 3. The temporal variation of the second moment of density $\langle\rho^2\rangle$ for the granular gas is shown for different values of σ for $\delta=0.001$. The curve with power $\langle\rho^2\rangle\sim t^{2/3}$ overlaps with all the data for $t_c<t<t_1$. The crossover time t_1 increases with decreasing σ, and is finite for $\sigma=\infty$.

extended patches reappearing, along with large white gaps, implying fragmentation of some large clusters and growth of smaller clusters. This is the signature of fluctuation dominated phase ordering.

The above picture can be quantified by measuring the second moment of the density distribution $\langle\rho^2\rangle$. For the sticky gas, it is known that $\langle\rho^2\rangle\sim t^{2/3}$ for $t\gg 1$. Does $\langle\rho^2\rangle$ in granular gas behave as that of sticky gas? Since there are three parameters σ, δ, and r_0 in the model, we need to carefully address the case with respect to varying these parameters.

Figure 2 shows the variation of $\langle\rho^2\rangle(t)$ with time t for varying δ, with $\sigma=3.0$ and $r_0=0.5$ fixed. The trends are the same for other values of σ. For early times $t_c<t<t_1$, $\langle\rho^2\rangle\sim t^{2/3}$ and completely overlaps with the same data for the sticky gas (shown by a line). For late times $t\gg t_1$, $\langle\rho^2\rangle$ deviates from the sticky gas behavior, the crossover occurring later for smaller δ (see Fig. 2). The quantitative dependence of the crossover time t_1 on δ can be obtained by collapsing the different curves by scaling. The collapse is excellent (see inset of Fig. 2) when the different curves and t are scaled as

$$\langle\rho^2\rangle=\frac{1}{\delta^{2/3}}f_1(t\delta). \tag{3}$$

Hence, we conclude that $t_1\sim\delta^{-1}$.

The crossover time t_1 also depends on σ. Figure 3 shows the variation of $\langle\rho^2\rangle$ with time t for different values of σ, keeping δ fixed at 0.001 and $r_0=0.5$. As earlier, for intermediate times the behavior of $\langle\rho^2\rangle$ mimics that of the sticky gas, while for large times, there is deviation beyond a scale t_1. The crossover time increases with decreasing σ. When $\sigma=\infty$, t_1 is finite but nonzero. Thus, we conclude that for all values of σ, the crossover time t_1 is finite and nonzero. Finally, we have checked that for fixed δ and σ, curves of $\langle\rho^2\rangle$ do not vary with r_0, thus implying that t_1 does not depend on r_0.

The coarsening behavior for times $t\gg t_1$ was discussed extensively in Ref. [27]. In this paper, we restrict ourselves to the regime $t_c<t<t_1$, and compare the coarsening behavior of granular gas to that of sticky gas. We bring out the similarities of the two through extensive simulations, the results of which are given below.

V. COMPARISON OF GRANULAR GAS TO STICKY GAS

In this section, we present results for granular gas and sticky gas for the intermediate times $t_c<t<t_1$. We show that they compare very well, and thus conclude strongly in favor of the equivalence of the two in this time regime. The following quantities are studied: the density distribution $P(\rho,t)$, the occupied cluster distribution $O(x,t)$, the empty interval distribution $E(x,t)$, density-density correlations $C_{\rho\rho}(r,t)$ (in real space), and $S_{\rho\rho}(k,t)$ (in Fourier space) and the velocity-velocity correlations $C_{vv}(r,t)$. For the sticky gas, the scalings of these distribution functions are known exactly through the exact solution in Ref. [4] and earlier studies [13]. However, some of the results, for example the velocity-velocity correlations, are complicated expressions whose behavior is not easily visualized. In addition, no plots are provided for ready reference. For completeness and future reference, we present numerical data for the sticky gas generated from event driven simulations. The results are, of course, in agreement with Refs. [4,13].

A. Density distribution function

The mass or density distribution for the sticky gas is a power law with a cutoff increasing with time, and an amplitude that decreases with time [4]. For sticky gas, it has the scaling form

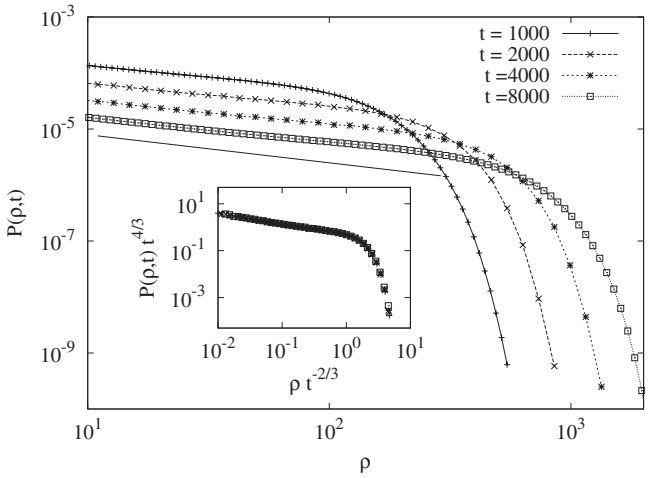

FIG. 4. The variation of $P(\rho,t)$ with ρ is shown for different times for the sticky gas. The straight line has an exponent $-1/2$. The inset shows the data collapse when scaled as in Eq. (4).

$$\lim_{L\to\infty} P(\rho,t) = \frac{1}{t^{4/3}} f_1\left(\frac{\rho}{t^{2/3}}\right), \tag{4}$$

where the scaling function $f_1(z) \sim 1/\sqrt{z}$ when $z \ll 1$ and $f_1(z) \to 0$ when $z \gg 1$. Thus, for densities much smaller than the cutoff $P(\rho,t) \sim (t\sqrt{\rho})^{-1}$. The simulation results for the sticky gas are shown in Fig. 4 for different times t. The data shows a time dependent cutoff, and power law with exponent $-1/2$. The scaling behavior is consistent with Eq. (4) (see inset of Fig. 4).

Now, consider granular gas for $t_c < t < t_1$. The variation of the density distribution $P(\rho,t)$ with ρ for different times is shown in Fig. 5. The distribution is a power law with the cutoff increasing with time and the amplitude decreasing with time. The cutoff scales exactly as in the case of sticky gas, i.e., $\rho_{\max} \sim t^{2/3}$. A good data collapse (shown in the inset of Fig. 5) is obtained when the different data are scaled as in Eq. (4).

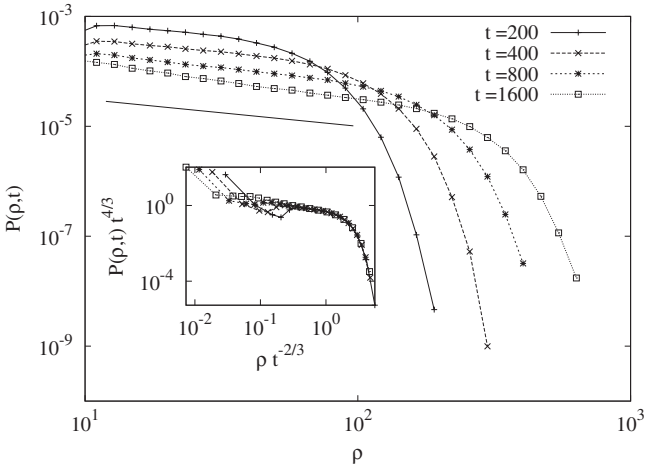

FIG. 5. The variation of the density distribution $P(\rho,t)$ with density ρ is shown for different times (in the early time regime) for granular gas. The straight line has an exponent -0.5. The inset shows the data collapse when scaled as in Eq. (4).

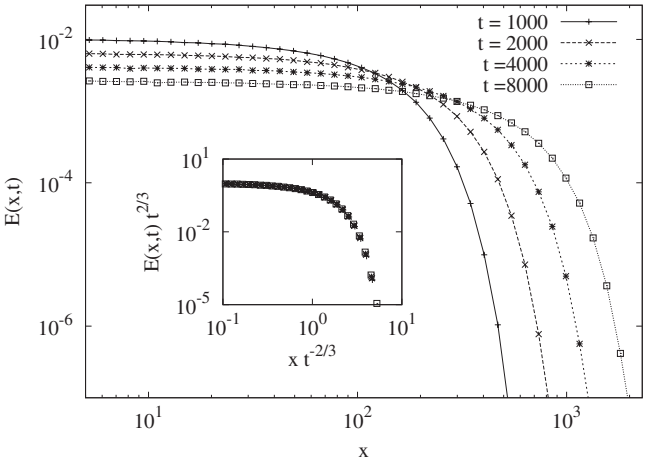

FIG. 6. The variation of the empty interval distribution $E(x,t)$ with separation x is shown for the sticky gas at different times. The inset shows the collapse of the curves when scaled as in Eq. (5).

We note that if $\delta \to 0$ the behavior of $P(\rho,t)$ as in Fig. 5 would continue indefinitely in time just as in sticky gas. But, in a more realistic granular gas model with finite δ, for $t \gg t_1$, the behavior of $P(\rho,t)$ completely changes and a new scaling function emerges asymptotically as was detailed in Ref. [27].

B. Empty and occupied cluster distribution functions

A suitable measure of clustering in space is the empty gap distribution $E(x,t)$. For sticky gas it is known [4] that

$$E(x,t) = \frac{1}{t^{2/3}} f_2\left(\frac{x}{t^{2/3}}\right), \tag{5}$$

where the scaling function $f_2(z) \to \text{const}$ when $z \to 0$ and $f_2(z) \to 0$ when $z \gg 1$. Thus, the largest empty cluster sizes $x_{\max} \sim t^{2/3}$. The simulation data for $E(x,t)$ for sticky gas is plotted in Fig. 6 for various times. The increasing cutoff points to the steady increase in the size of empty clusters, as is usual in phase ordering systems. The decreasing amplitude of the distribution for small sizes indicate that small empty gaps are steadily disappearing from the system with time. In the inset of Fig. 6, the data collapse is shown following Eq. (5).

For granular gas, the scaling and shape of the scaling function for $E(x,t)$ matches that of sticky gas well. In Fig. 7 we present the data for various times and in the inset the scaling collapse using Eq. (5). The collapse is excellent, showing the equivalence of granular gas to sticky gas as far as $E(x,t)$ is concerned.

It turns out that in granular gas for $t \gg t_1$, the above clean phase ordering behavior of $E(x,t)$ dramatically changes and a power law distribution for the scaling function $f_2(z)$ appears with a large negative power (≈ 2.2) [27], signaling a crossover to fluctuation dominated phase ordering behavior. The occupied cluster distribution $O(x,t)$, has a very different form and evolution in comparison to $E(x,t)$ discussed above. In the absence of any analytical guidance on this quantity from earlier works on sticky gas, we present directly what

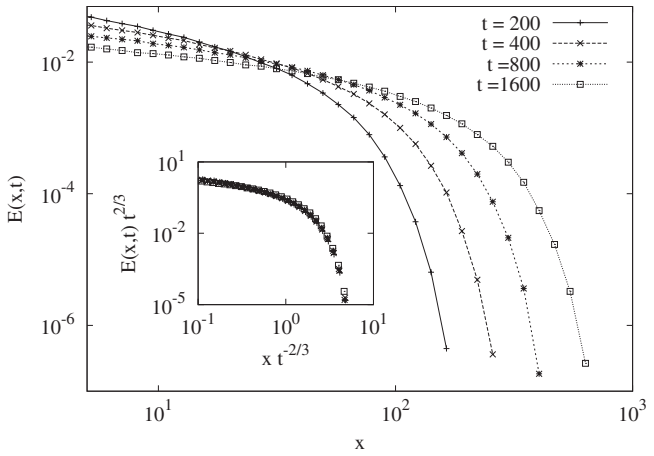

FIG. 7. The variation of the empty interval distribution $E(x,t)$ with separation x is shown for the granular gas at different times. The inset shows the collapse of the curves when scaled as in Eq. (5).

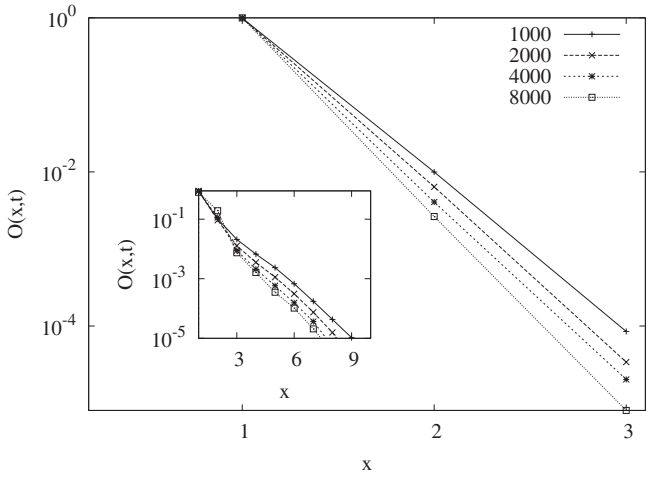

FIG. 8. The variation of the occupied cluster length distribution $O(x,t)$ with separation x, is shown at different times for the sticky gas on a linear-log plot. Inset: A similar plot for the granular gas. The times are $t=200$ (top curve), 400, 800, and 1600 (bottom curve).

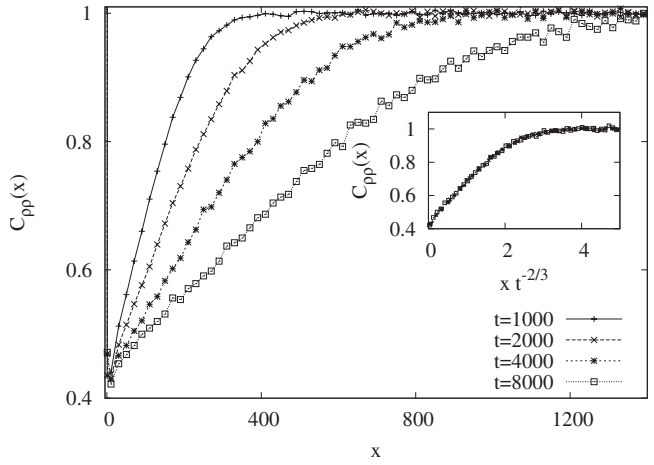

FIG. 9. The density-density correlation function $C_{\rho\rho}$ as a function of x for the sticky gas. Inset: The data collapse when scaled as in Eq. (6).

we find in our simulation. The data for $O(x,t)$ is shown in Fig. 8. We see that large occupied clusters are extremely rare, and within size 3 the distribution fall to very low value. The distribution function $O(x,t)$ is exponential with x, and its width decreases marginally with time. Thus, we conclude that occupied clusters are highly localized in space and do not vary much in time.

In the inset of Fig. 8, we show $O(x,t)$ for granular gas in the early time regime. The curves are strikingly similar to sticky gas. There is an exponential decay over very short sizes, and clusters beyond size 9 are very rare. Again there is a marginal decrease in width of the distribution with time. Just as the sticky gas, this implies extremely localized occupied clusters, whose width do not vary appreciably with time.

We note that, in sharp contrast to the above scenario, the occupied clusters do not remain localized at large times $t \gg t_1$ for granular gas. In fact $O(x,t)$ also decays as a power law similar to $E(x,t)$ with the same negative power (≈ 2.2) as was shown in Ref. [27].

C. Density-density correlation functions

The two point spatial correlation functions give a very vivid picture of the type of phase ordering that the system undergoes, and we discuss these in this and the next subsection. The data for two point density-density correlation function $C_{\rho\rho}$ (defined in Sec. III) of sticky gas is plotted in Fig. 9. The correlation function drops from a very large value at $x=0$ to a value below 1 and then asymptotically increases to 1 as $x \to \infty$. The initial drop is because near every particle there is a density depletion zone created by coalescence of clusters. The asymptotic approach is expected as $C_{\rho\rho} \to \langle \rho \rangle^2$ for large x and $\langle \rho \rangle = 1$. For a phase ordering system [35] the scaling form

$$C_{\rho\rho}(x,t) = f_3(x/\mathcal{L}) \tag{6}$$

is expected and we show the data collapse in the inset of Fig. 9. For small scaled distance $x/\mathcal{L}$, the scaling function f_3 increases linearly, implying that the Porod law [36] is valid.

The corresponding data for $C_{\rho\rho}$ for the granular gas at intermediate times is shown in Fig. 10. We find a striking similarity between Figs. 10 and 9 (for the sticky gas). The scaling function shown in the inset of Fig. 10 is very similar to the inset in Fig. 9.

To find the structure function $S_{\rho\rho}(k,t)$ which scales in the conventional fashion one has to treat the data for $C_{\rho\rho}(x,t)$ carefully. First, the value at $x/\mathcal{L}=0$ for the scaled $C_{\rho\rho}(x,t)$ do not form a part of the scaling function f_3 and have to be carefully adjusted by hand so as not to introduce undesirable distortions in k space. This procedure has been discussed in details in Ref. [37], and we do the same in this case. Secondly, $f_3(z)$ does not decay to zero at $z \to \infty$ and well behaved Fourier transform cannot be found. So for this special case of the density-density correlation function for both the sticky and the granular gases, we define $S_{\rho\rho}(k,t)$ to be the Fourier

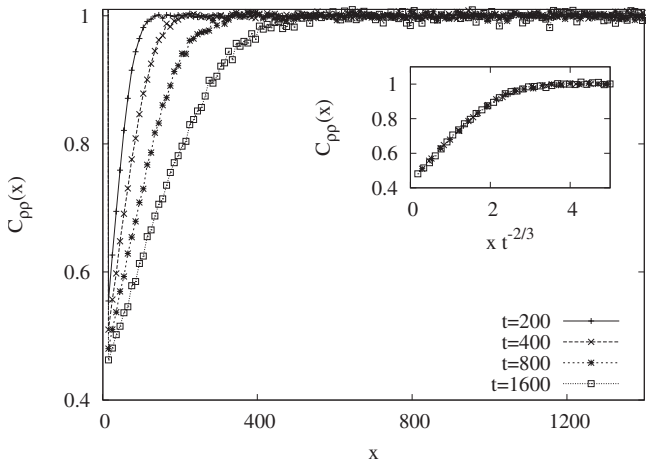

FIG. 10. The density-density correlation function $C_{\rho\rho}$ as a function of x for the granular gas. Inset: The data collapse when scaled as in Eq. (6).

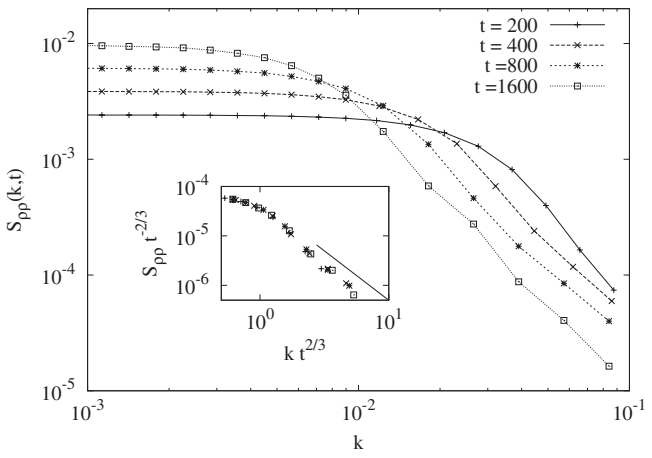

FIG. 12. The variation of $S_{\rho\rho}$ with k is shown for the granular gas at early times. The inset shows the data collapse when scaled as in Eq. (7). The straight line has an exponent −2.0.

transform of $1-C_{\rho\rho}(x,t)$. The latter real space function nicely decays to zero at large x and thus $S_{\rho\rho}(k,t)$ is expected to be well behaved. The data thus obtained are shown in Fig. 11 for the sticky gas, and in Fig. 12 for the granular gas (for small times). They compare very well, and in the insets of Figs. 11 and 12, the scaling collapse of the data are shown according to

$$S_{\rho\rho}(k,t) = \mathcal{L} g_3[k\mathcal{L}(t)]. \tag{7}$$

For large $k\mathcal{L}$ we see that for both sticky and granular gas the scaling function $g_3(z) \sim z^{-2}$ for $z \gg 1$, i.e., obey the Porod law, as is expected for a clean phase ordering system.

For times $t \gg t_1$ there is a shift to non-Porod behavior for granular gas as discussed in Ref. [27]. The functional form of $g_3(x)$ completely changes in that regime.

D. Velocity-velocity correlation functions

The velocity-velocity correlation function C_{vv} is expected [27] to scale as $\sim(v_t/\mathcal{L})^2 f_4(x/\mathcal{L})$, where v_t is the typical velocity which scales as $t^{-1/3}$, and the factor $1/\mathcal{L}$ accounts for probability of a box being occupied. The scaling function $f_4(x)$ decays to zero for large x. Putting in the t dependence for v_t and $\mathcal{L}$, we obtain

$$C_{vv}(x,t) = \frac{1}{t^2} f_4(x/\mathcal{L}). \tag{8}$$

In Fig. 13, the data for $C_{vv}(x,t)$ at different times is shown for sticky gas. The inset shows the data collapse when scaled as in Eq. (8). The scaling function $f_4(z)$ decays linearly for small z and goes to zero for large z. The linearity is again a clear signature of the Porod law.

The corresponding data for $C_{vv}(x,t)$ for granular gas is shown in Fig. 14. There are corrections to scaling when compared to the corresponding data for sticky gas (see inset of Fig. 14). A possible reason is that the times for which the measurements are taken for granular gas are a factor of 10 smaller that of sticky gas. However, it is seen (see inset of Fig. 14) that, for increasing time, the $x/\mathcal{L}$ at which deviation

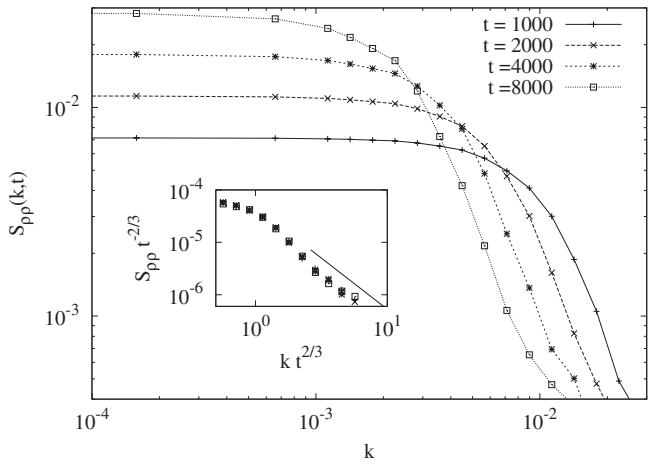

FIG. 11. The variation of $S_{\rho\rho}$ with k for the sticky gas is shown for different times. The inset shows the data collapse when scaled as in Eq. (7). The straight line has an exponent −2.0.

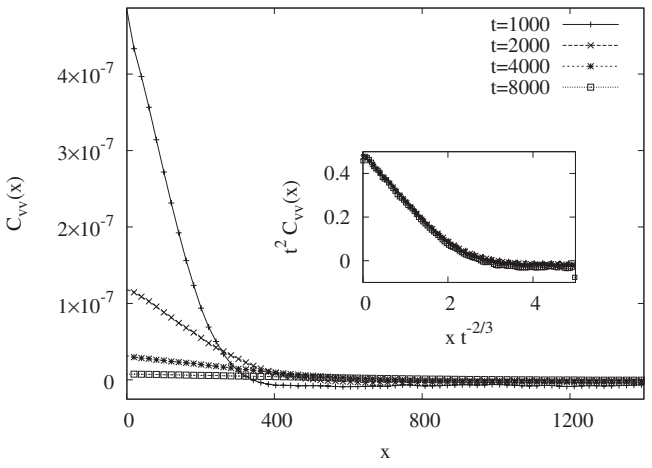

FIG. 13. The figure shows the variation of $C_{vv}(x,t)$ with x for different times. The data is for the sticky gas. The inset shows the data collapse when scaled as in Eq. (8).

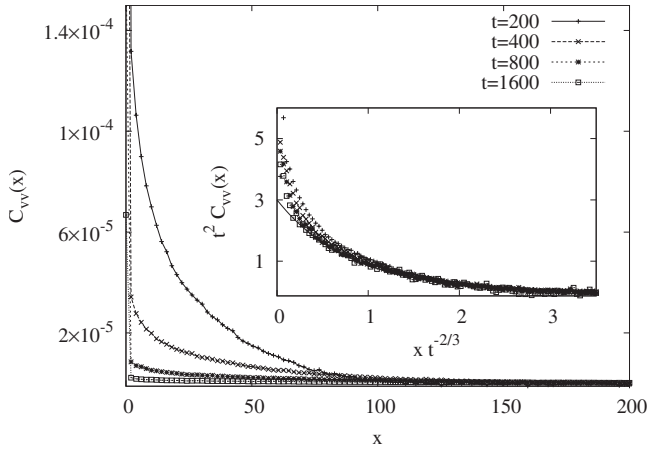

FIG. 14. The figure shows the variation of $C_{vv}(x,t)$ with x for different times for the granular gas. The inset shows the curves when scaled as in Eq. (8). The higher curves correspond to smaller times. At large times, the data approaches the solid line, an exponential obtained by fitting the scaling region.

from scaling occurs decreases. The scaling function tends towards the curve $3.0\exp(-1.25x/\mathcal{L})$ (drawn as a solid line in the inset of Fig. 14). Thus, again a linear decay is obtained near the origin, signifying Porod law. The scaling functions in the inset of Figs. 13 and 14 differ by a factor of 6 for small $x/\mathcal{L}$. This is probably a consequence of the coarsening rule that we have used.

We also note that the structure function $S_{vv}(k,t)$, obtained as the Fourier transform of $C_{vv}(x,t)$, should scale as

$$S_{vv}(k,t) = \frac{1}{t^{4/3}} g_4(k\mathcal{L}). \tag{9}$$

However, due to corrections to scaling for small $x/\mathcal{L}$, we cannot obtain good data for large k, and hence we do not show the structure functions as plots.

VI. THE INDEPENDENT INTERVAL APPROXIMATION

In this section, starting from the empty and occupied interval distributions, we derive the Porod law for density-density correlations via a mean-field approximation, often referred to as independent interval approximation [42]. This approximation was used in Ref. [27] to connect the interval distributions to the density correlations for times $t \gg t_1$. Here, we first give the derivation of the result used in Ref. [27], and then apply it to times $t_c < t < t_1$.

The equal time density-density correlation function $C_{\rho\rho}(x) = \langle \rho_i(t)\rho_{i+x}(t)\rangle$ is the expectation value of the product of densities of boxes separated by spatial distance x. This quantity can be estimated using an approximation which is discussed below. Let $p_k(x)$ denote the probability that given that site 0 is occupied, there are exactly $1+[k/2]$ occupied intervals and $[(k+1)/2]$ empty intervals, where $[\cdots]$ denotes the integer part. An example of configurations contributing to p_k is shown in Fig. 15(a) for odd $k=2n-1$ and Fig. 15(b) for even $k=2n$. Thus, $p_0(x)$ will correspond to the situation when 0 is occupied and there is continuous set of occupied sites up

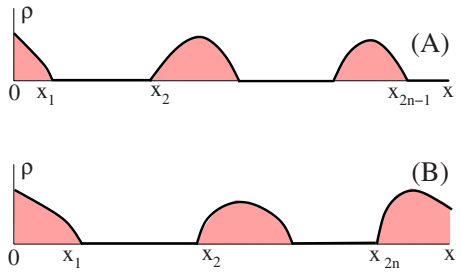

FIG. 15. (Color online) A schematic diagram showing configurations that contribute to p_k when $k=2n-1$ is odd (a) and when $k=2n$ is even (b). The shaded regions represent boxes with nonzero density ρ. The even k correspond to the case when both the sites 0 and x are occupied and contribute to the density-density correlation function $C_{\rho\rho}(x,t)$.

to x, while $p_1(x)$ would correspond to a set of occupied sites starting from 0, followed by an empty interval extending beyond x. Since $C_{\rho\rho}(x)$ is approximately equal to density square times the probability that there is a nonzero density at x given there is a nonzero density at 0, we obtain (setting $\rho=1$)

$$C_{\rho\rho}(x) \approx \sum_{n=0}^{\infty} p_{2n}(x), \tag{10}$$

where $p_{2n}(x)$ is the probability of having exactly n empty gaps between 0 and x with 0 and x being occupied.

The probabilities $p_k(x)$ may be expressed in terms of the gap distributions $E(x,t)$ and $O(x,t)$. Let

$$Q(x,t) = \int_x^{\infty} dx' O(x',t), \tag{11}$$

$$F(x,t) = \int_x^{\infty} dx' E(x',t), \tag{12}$$

where $Q(x,t)$ is the probability of getting an occupied cluster of size greater than x. Similarly $F(x,t)$ is the probability of getting an empty cluster of size greater than x.

Approximating joint distributions $p_{2n}(x)$ and $p_{2n-1}(x)$ by products of individual distributions of the intervals (namely, E, O, Q, and F), one can easily verify (following Fig. 15 as a guideline for the odd and the even cases), that

$$p_{2n-1}(x) = \alpha \int dx_1 \cdots dx_{2n-1} Q(x_1) F(x - x_{2n-1}) \times \prod_{j=1,3,\ldots}^{2n-3} [E(x_{j+1} - x_j) O(x_{j+2} - x_{j+1})], \quad n = 1,2,\ldots, \tag{13}$$

$$p_{2n}(x) = \alpha \int dx_1 \cdots dx_{2n} Q(x_1) E(x_{2n} - x_{2n-1}) Q(x - x_{2n}) \times \prod_{j=1,3,\ldots}^{2n-3} [E(x_{j+1} - x_j) O(x_{j+2} - x_{j+1})], \quad n = 1,2, \ldots, \tag{14}$$

$$p_0(x) = \alpha \int dx' Q(x'), \tag{15}$$

where α is a normalization constant that will be determined shortly. Equations (13)–(15) simplify considerably if we take Laplace transforms. Denoting the Laplace transform of a function $f(x)$ by $\tilde{f}(s)$, where $\tilde{f}(s) = \int_0^\infty f(x) e^{-sx} dx$, we obtain

$$\tilde{p}_{2n-1}(s) = \alpha \tilde{Q} \tilde{F} (\tilde{E}\tilde{O})^{n-1}, \quad n = 1,2, \ldots, \tag{16}$$

$$\tilde{p}_{2n}(s) = \alpha \tilde{Q}^2 \tilde{E} (\tilde{E}\tilde{O})^{n-1}, \quad n = 1,2, \ldots, \tag{17}$$

$$\tilde{p}_0(s) = \frac{\alpha}{s} [\langle x \rangle_0 - \tilde{Q}], \tag{18}$$

where $\langle x \rangle_0 = \int_0^\infty dx x O(x)$ is the mean length of an occupied cluster. The distribution $\tilde{Q}(s)$ can be expressed in terms of the probability density $\tilde{O}(s)$ as

$$\tilde{Q}(s) = \frac{1}{s} [1 - \tilde{O}(s)] \tag{19}$$

and likewise for $\tilde{F}$ [with $\tilde{O}$ replaced in Eq. (19) by $\tilde{E}$]. The constant α can now be determined from the condition $\Sigma_{n=0}^\infty \tilde{p}_n(s) = s^{-1}$, which follows from $\Sigma_{n=0}^\infty p_n(x) = 1$. We immediately obtain $\alpha = 1/\langle x \rangle_o$. Equations (10), (16), (18), and (19) give

$$\tilde{C}_{\rho\rho}(s) = \frac{1}{s} - \frac{[1 - \tilde{O}(s)][1 - \tilde{E}(s)]}{\langle x \rangle_o s^2 [1 - \tilde{E}(s)\tilde{O}(s)]}. \tag{20}$$

We now need the form of $\tilde{O}(s,t)$ and $\tilde{E}(s,t)$. The occupied cluster size distribution $O(x,t)$ has no dependence on the length scale $\mathcal{L}(t)$ (see Fig. 8). The distribution is very close to a pure exponential and we take it to be of the form $O(x,t) \approx a^{-1} \exp(-x/a)$, where a is independent of time. Then $\tilde{O}(s,t) \approx (as+1)^{-1}$. The empty interval distribution $E(x,t)$ is a constant for small x and goes to zero for $x \gg L_t$ (see Figs. 6 and 7). We approximate it by a step function $E(x,t) = \mathcal{L}_t^{-1}$ for $x \leqslant \mathcal{L}_t$, and $E(x,t) = 0$ for $x > \mathcal{L}_t$. Then, $\tilde{E}(s,t) \approx (s\mathcal{L}_t)^{-1} [1 - \exp(-s\mathcal{L}_t)]$.

We are interested in the limit $s \to 0$, $\mathcal{L} \to \infty$ keeping $s\mathcal{L}$ a constant. For verifying the Porod law, we are further interested in the limit $s\mathcal{L} \gg 1$. Substituting the assumed forms for $\tilde{E}$ and $\tilde{O}$ in Eq. (20) and expanding for large $s\mathcal{L}$, we obtain

$$\frac{C_{\rho\rho}(s)}{\mathcal{L}} \approx \frac{1}{(s\mathcal{L})^2}, \quad s\mathcal{L} \gg 1. \tag{21}$$

We thus obtain the Porod law behavior by using the cluster distributions. The same independent interval approximation gives consistent results between the cluster distributions and the two point correlation functions in late time regime $t > t_1$ [27], where there is a violation of Porod law.

VII. SUMMARY AND CONCLUSIONS

In this paper, we studied the density distribution, the empty and occupied cluster distributions, the spatial density-density correlations, and the velocity-velocity correlations in granular gas undergoing inelastic collisions in one dimension. The restitution coefficient was modeled as being velocity dependent, with the collisions becoming nearly elastic when the relative velocity is less than a velocity scale δ. The velocity scale δ introduced a new time scale t_1 into the problem. In this paper, the dependence of t_1 on the different parameters was found. Due to the existence of t_1, and the crossover scale t_c between the homogeneous and inhomogeneous cooling regimes, there are three different time regimes in the problem: (1) $t < t_c$, during which particles undergo homogeneous cooling, (2) $t_c < t < t_1$, referred to as intermediate times, and (3) $t > t_c$ referred to as late times. In this paper, the focus was on the intermediate times.

For intermediate times, we compared the different correlation functions of granular gas with that of sticky gas. We found that there is an excellent match between the two. Coarsening in both the cases is governed by the Porod law. These results thus support the claim that the Burgers equation is the correct description for granular gas [5].

For late times, this equivalence breaks down [27]. The coarsening in the granular gas violates the Porod law. The occupied cluster distribution and the empty cluster distributions differ significantly from intermediate times by developing into power laws. The existence of clusters of all sizes leads to fluctuation dominated coarsening. A continuum equation describing this regime is missing, and it would be interesting to find one in future.

ACKNOWLEDGMENTS

We thank M. Barma for useful discussions. D.D. was supported by Grant No. 3404-2 of "Indo-French Center (IFCPAR)/(CEFIPRA)."

[1] H. M. Jaeger, S. R. Nagel, and R. P. Behringer, Rev. Mod. Phys. **68**, 1259 (1996).
[2] L. Kadanoff, Rev. Mod. Phys. **71**, 435 (1999).
[3] I. S. Aranson and L. S. Tsimring, Rev. Mod. Phys. **78**, 641 (2006).
[4] L. Frachebourg, Phys. Rev. Lett. **82**, 1502 (1999).
[5] E. Ben-Naim, S. Y. Chen, G. D. Doolen, and S. Redner, Phys. Rev. Lett. **83**, 4069 (1999).

[6] X. Nie, E. Ben-Naim, and S. Chen, Phys. Rev. Lett. **89**, 204301 (2002).
[7] C. Cattuto and U. M. B. Marconi, Phys. Rev. Lett. **92**, 174502 (2004).
[8] S. Das and S. Puri, Phys. Rev. E **68**, 011302 (2003).
[9] A. Baldassarri, U. M. B. Marconi, and A. Puglisi, Europhys. Lett. **58**, 14 (2002).
[10] A. Baldassarri, U. M. B. Marconi, and A. Puglisi, Phys. Rev. E **65**, 051301 (2002).
[11] S. Ostojic, D. Panja, and B. Nienhuis, Phys. Rev. E **69**, 041301 (2004).
[12] G. F. Carnevale, Y. Pomeau, and W. R. Young, Phys. Rev. Lett. **64**, 2913 (1990).
[13] S. Kida, J. Fluid Mech. **93**, 337 (1979).
[14] A. Puglisi, V. Loreto, U. M. B. Marconi, A. Petri, and A. Vulpiani, Phys. Rev. Lett. **81**, 3848 (1998).
[15] A. Puglisi, V. Loreto, U. Marini Bettolo Marconi, and A. Vulpiani, Phys. Rev. E **59**, 5582 (1999).
[16] E. Trizac and J.-P. Hansen, Phys. Rev. Lett. **74**, 4114 (1995).
[17] E. Trizac and A. Barrat, Eur. Phys. J. E **3**, 291 (2000).
[18] A. Barrat, T. Biben, Z. Racz, E. Trizac, and F. van Wijland, J. Phys. A **35**, 463 (2002).
[19] Sean McNamara and W. R. Young, Phys. Rev. E **53**, 5089 (1996).
[20] I. Goldhirsch and G. Zanetti, Phys. Rev. Lett. **70**, 1619 (1993).
[21] O. Petzschmann, U. Schwarz, F. Spahn, C. Grebogi, and J. Kurths, Phys. Rev. Lett. **82**, 4819 (1999).
[22] T. P. C. van Noije, M. H. Ernst, R. Brito, and J. A. G. Orza, Phys. Rev. Lett. **79**, 411 (1997).
[23] J. Javier Brey, F. Moreno, and M. J. Ruiz-Montero, Phys. Fluids **10**, 2965 (1998).
[24] P. Haff, J. Fluid Mech. **134**, 401 (1983).
[25] C. C. Maaβ, N. Isert, G. Maret, and C. Aegerter, Phys. Rev. Lett. **100**, 248001 (2008).
[26] J. M. Burgers, *The Non-Linear Diffusion Equation: Asymptotic Solutions and Statistical Problems* (Reidel, Boston, 1974).
[27] M. Shinde, D. Das, and R. Rajesh, Phys. Rev. Lett. **99**, 234505 (2007).
[28] C. V. Raman, Phys. Rev. **12**, 442 (1918).
[29] L. Labous, A. D. Rosato, and R. N. Dave, Phys. Rev. E **56**, 5717 (1997).
[30] E. Falcon, C. Laroche, S. Fauve, and C. Coste, Eur. Phys. J. B **3**, 45 (1998).
[31] R. Ramírez, T. Pöschel, N. V. Brilliantov, and T. Schwager, Phys. Rev. E **60**, 4465 (1999).
[32] N. Brilliantov, C. Salueña, T. Schwager, and T. Pöschel, Phys. Rev. Lett. **93**, 134301 (2004).
[33] J. J. Brey, D. Cubero, and M. J. Ruiz-Montero, Phys. Rev. E **59**, 1256 (1999).
[34] N. V. Brilliantov and T. Pöschel, Phys. Rev. E **61**, 5573 (2000).
[35] A. J. Bray, Adv. Phys. **43**, 357 (1994).
[36] G. Porod, *Small-Angle X-ray Scattering* (Academic, London, 1982).
[37] D. Das, M. Barma, and S. N. Majumdar, Phys. Rev. E **64**, 046126 (2001).
[38] G. Manoj and M. Barma, J. Stat. Phys. **110**, 1305 (2003).
[39] A. Nagar, M. Barma, and S. N. Majumdar, Phys. Rev. Lett. **94**, 240601 (2005).
[40] S. Mishra and S. Ramaswamy, Phys. Rev. Lett. **97**, 090602 (2006).
[41] E. Thiesen and W. A. M. Morgado, Phys. Rev. E **73**, 051303 (2006).
[42] S. N. Majumdar, C. Sire, A. J. Bray, and S. J. Cornell, Phys. Rev. Lett. **77**, 2867 (1996).